Separation Science and Technology
Publication details, including instructions for authors and subscription information:
http://www.informaworld.com/smpp/title~content=t713708471

Analysis and Simulation of Hollow-Fiber Reverse-Osmosis Modules

Amal M. El-Halwagi[a]; Vasilios Manousiouthakis[a]; Mahmoud M. El-Halwagi[b]
[a] CHEMICAL ENGINEERING DEPARTMENT, UNIVERSITY OF CALIFORNIA, LOS ANGELES, LOS ANGELES, CALIFORNIA, USA [b] CHEMICAL ENGINEERING DEPARTMENT, AUBURN UNIVERSITY, AUBURN, ALABAMA, USA

To cite this Article El-Halwagi, Amal M. , Manousiouthakis, Vasilios and El-Halwagi, Mahmoud M.(1996) 'Analysis and Simulation of Hollow-Fiber Reverse-Osmosis Modules', Separation Science and Technology, 31: 18, 2505 — 2529
To link to this Article: DOI: 10.1080/01496399608001062
URL: http://dx.doi.org/10.1080/01496399608001062

SEPARATION SCIENCE AND TECHNOLOGY, 31(18), pp. 2505–2529, 1996

Analysis and Simulation of Hollow-Fiber Reverse-Osmosis Modules

AMAL M. EL-HALWAGI and VASILIOS MANOUSIOUTHAKIS
CHEMICAL ENGINEERING DEPARTMENT
UNIVERSITY OF CALIFORNIA, LOS ANGELES
LOS ANGELES, CALIFORNIA 90024, USA

MAHMOUD M. EL-HALWAGI
CHEMICAL ENGINEERING DEPARTMENT
AUBURN UNIVERSITY
AUBURN, ALABAMA 36849, USA

ABSTRACT

The purpose of this work is to analyze the performance of hollow-fiber reverse-osmosis (HFRO) systems. First, the mass and momentum balances on the fluids inside and outside of the hollow fibers are derived. Consequently, these equations are coupled with the membrane transport expressions to provide a two-phase model for completely describing the hydrodynamic behavior of HFRO units. The model equations are solved numerically via discretization techniques. Experimental data are used for two objectives; transport-parameters estimation and model validation. Based upon optimization principles, a parameter-estimation technique is proposed for correlating the membrane-transport coefficients with the operating pressures and concentrations. The model validity is elucidated by comparing the theoretical predictions with the experimental data for different HFRO modules and over a wide range of operating parameters.

INTRODUCTION

Recently, there has been a growing industrial interest in using reverse osmosis for several objectives such as water purification and demineralization as well as environmental applications (e.g., Refs. 2 and 24). In particular, hollow-fiber reverse-osmosis "HFRO" systems have received considerable attention as an effective separation technique. Among the different

configurations of semipermeable membranes used for reverse osmosis, the hollow-fiber modules have a number of distinguishing characteristics such as the large surface-to-volume ratio, the self-supporting strength of fibers, and the negligible concentration polarization near the membrane surface. A hollow-fiber reverse-osmosis module (see Fig. 1) consists of a shell which houses the hollow fibers. The fibers are grouped together in a bundle with one end sealed and the other open to the atmosphere. The open ends of the fibers are potted into an epoxy sealing head plate after which the permeate is collected. The pressurized feed solution (denoted by the shell-side fluid) flows radially from a central porous tubular distributor. As the feed solution flows around the outer side of the fibers toward the shell perimeter, the permeate solution penetrates through the fiber wall into the bore side by virtue of reverse osmosis. The permeate is collected at the open ends of the fibers. The reject solution is collected at the porous wall of the shell.

The development of a reliable mathematical model for the description of HFRO systems is a highly desirable goal. First, it serves as a powerful tool for analyzing the transport properties of hollow-fiber membranes. To date, very few research works have been devoted to the estimation of transport parameters of HFRO units. Owing to the strong interaction between the hydrodynamic characteristics and the transport parameters of the system, the values of the transfer coefficients reported in literature have varied considerably. Clearly, the accuracy of these coefficients is strictly related to the validity of the hydrodynamic model of the system. In this context, Pusch (22) states that "Regarding the determination of intrinsic transport parameters of hollow fibers, the following should be

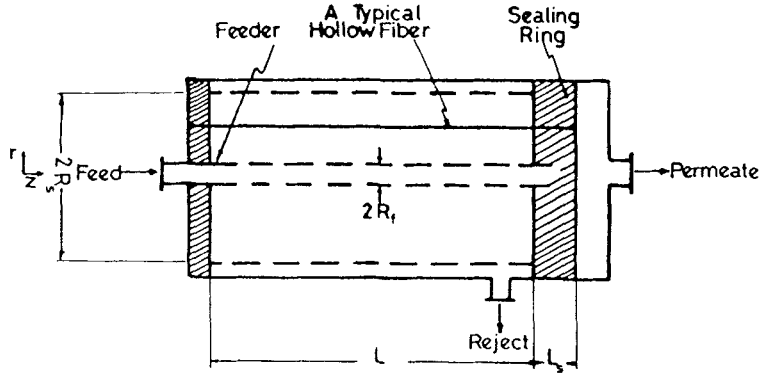

FIG. 1 Schematic representation of the HFRO module.

said. In order to rigorously treat the hydrodynamics inside hollow fibers, the Navier-Stokes equations and deformation equations of the fibers must be solved simultaneously. No complete integral of this complex system of differential equations is available from the literature although there exist several approximate solutions for special limiting cases." A second objective of developing a realistic hydrodynamic model is to establish a systematic framework for optimizing the design of new HFRO units or improving the performance of already existing units by invoking the optimal operating conditions. Since HFRO systems are typically arranged in networks of several units, the developed model represents an essential part of any optimal network-synthesis methodology.

In recent years a number of mathematical models have been devised to simulate the hydrodynamic performance of HFRO modules. In these models, two approaches have been generally adopted to estimate the pressure variation through the shell side. In the first approach, the shell-side pressure is assumed to be constant (9, 18, 27). The second approach treats the fiber bundle as a porous medium and describes the flow through this medium by Darcy's equation with an arbitrary empirical constant (3, 11, 14, 19). The value of the empirical constant is strictly applicable to the geometry and operating conditions for which it has been evaluated. As a result of the pressure drop inside the fibers along the module, the pressure difference across the fiber wall may vary significantly and, thus, the permeation rate may change considerably along the fiber length. Therefore, an axial component of the shell-side flow arises in addition to the radial component. It should be pointed out that the existing models for radial-flow hollow-fiber systems assume a purely radial flow in the shell side. Apparently this assumption does not accurately reflect the shell-side flow distribution.

Owing to the above-mentioned limitations associated with existing models, none of them appears to provide a reliable description for the performance of HFRO systems over the whole range of industrial operating conditions. In characterizing the predictive power of existing models, Soltanieh and Gill (28) stated that: "Limited success has been achieved in predicting the model rejection coefficient for various feed conditions (concentration, pressure, flowrate, etc.)."

The present work aims at achieving several objectives. Based upon the fundamental transport equations, a mathematical model is devised to describe the hydrodynamic performance of HFRO systems. Next, an efficient numerical algorithm is developed to solve the model equations. Finally, numerous experimental data are used to estimate the membrane transport parameters and to test the validity of the devised model and transport parameters.

THEORETICAL ANALYSIS

In this section the model equations necessary for describing the behavior of HFRO units will be presented. Based upon the fundamental mass and momentum transport equations, a coupled two-phase model will be derived. The shell side will be treated as a continuous phase. This representation was first proposed by Gill and Bansal (8). It allows the use of a two-dimensional continuous model for the shell-side hydrodynamics. It also obviates the need for a discontinuous representation of flow whenever a fiber is encountered. As has been mentioned in the Introduction, while the bulk of the flow in the shell side is in the radial direction, an axial velocity may also develop due to the varying rates of permeation alongside the fibers. Therefore, the flow field in the shell side will be described by two velocity components; axial and radial.

Model Assumptions

1. The shell side is assumed to be an axially symmetric continuum in which the hollow fibers are considered to be uniformly distributed continuous sinks.
2. The shell side has negligible concentration polarization. The validity of this assumption was elucidated by Kabadi et al. (14) who showed that under typical operating conditions of HFRO units the wall concentration differs from that at the shell bulk by 1.4% at most.
3. Osmotic pressure is a linear function of salt concentration. This assumption is based upon the Van't Hoff equation which is most reliable for relatively dilute solutions. For high salt concentrations, experimental values or nonlinear models relating osmotic pressure to concentration ought to be used.
4. The membrane transport equations are given by the Kedem–Katchalsky model (15) as follows.

Water Flux

$$J_w = L_p(\Delta P - \sigma \Delta \pi) \tag{1}$$

where L_p is the filtration coefficient which provides a measure of the hydrodynamic permeability of the membrane to the solvent. The reflection coefficient, σ, indicates the extent of solute rejection by the membrane. When $\sigma = 0$, the membrane is totally permeable to the solute (no salt rejection). On the other hand, when the value of σ reaches 1, the membrane is completely impermeable to the solute (100% solute rejection).

By using Assumption 3 and rearranging, one may rewrite Eq. (1) as

$$J_w = L_p \left[\Delta P - \sigma \frac{\pi_0}{c_0} (c_1 - c_3) \right] \tag{2}$$

where π_0 and c_0 are any corresponding osmotic pressure and concentration for the particular salt under consideration.

Salt Flux

$$J_s = (c_s)_{\log \text{ mean}}(1 - \sigma)J_w + \omega \frac{\pi_0}{c_0} (c_1 - c_3) \tag{3}$$

Where both J_w and J_s are defined based on the outside surface of fiber. The term $(c_s)_{\log \text{ mean}}$ is the logarithmic average solute concentration across the membrane. Equation (3) implies that the solute flux is a combination of two trans-membrane flows; convective (with the solvent flux) and diffusive (due to concentration gradient). Hence, at zero solvent flux, Eq. (3) becomes

$$(J_s)_{\text{at } J_w = 0} = \omega \frac{\pi_0}{c_0} (c_1 - c_3) \tag{4}$$

which indicates that ω is a measure of the solute permeability of the membrane at zero solvent flux.

The model of Kedem and Katchalsky is used since its transport coefficients σ and ω are not very sensitive to variations in operating pressures and concentrations (26). Nonetheless, in Eqs. (1)–(4) the membrane-transport coefficients are allowed to be pressure- and concentration-dependent. The functional dependence of these parameters on pressure and concentration will be discussed later.

Model Equations

Shell-Side Continuity Equation

For an incompressible flow, the equation of continuity is given by

$$\nabla \cdot v = -Q \tag{5}$$

where Q is the volume of fluid entering the sink per unit shell volume per unit time and is related to the local permeation flux velocity through the membrane, J_w, by

$$Q = \frac{2(1 - \epsilon)}{r_0} J_w \tag{6}$$

Momentum-Balance Equations for the Shell Side

The vector form of the momentum-balance equation for the shell side may be written as

$$\frac{\partial \rho v}{\partial t} = -[\nabla \cdot \rho v v] - \nabla p - [\nabla \cdot \tau] \tag{7}$$

substituting from Eq. (5) into Eq. (7) and rearranging, we get

$$\rho \frac{Dv}{Dt} = -\nabla p - [\nabla \cdot \tau] + \rho Q v \tag{8}$$

in which the last term on the right-hand side accounts for the existence of the continuously distributed sinks and the operator D/Dt is the substantial time derivative.

In order to incorporate the effect of viscous drag forces exerted by the fluid on the outside surface of the swarm of fibers into Eq. (8), Brinkman's model (1) will be used, The essence of this model is that the fluid in proximity to an obstacle embedded in a porous medium experiences a body damping force in addition to the usual forces in the equation of motion. Brinkman suggested that the effect of this damping force may be incorporated into the equation of motion by adding Darcy's resistance term to the Navier–Stokes equation. This model has been successfully used in describing the hydraulics of flow through porous media and fibrous beds (e.g., Ref. 29). Tam (30) and Lundgren (17) gave rigorous theoretical justification of Brikman's model using a statistical approach. Therefore, by using Brinkman's analysis, Eq. (8) should be modified to the following form

$$\rho \frac{Dv}{Dt} = -\nabla p - [\nabla \cdot \tau] - \left[\frac{\mu}{k} - \rho Q\right] v \tag{9}$$

Another way of deriving Eq. (9) is by invoking the transport equation for a two-phase system. Based upon volume-averaging concepts (31) one can write the following momentum-balance equation for the shell-side fluids:

$$\rho \frac{Dv}{Dt} = -\nabla p - [\nabla \cdot \tau] - B + S(\bar{v} - v) \tag{10a}$$

in which B is the force per unit volume that the outside surface of the fibers exerts on the shell-side fluid. As has been previously discussed, according to Brinkman's analysis this damping force can be described by

$$B = \frac{\mu}{k} v \tag{10b}$$

The term S in Eq. (10a) represents the mass rate of consumption of the shell fluid (via permeation into the bore-side sink) per unit shell volume. According to our terminology

$$S = -\rho Q \tag{10c}$$

Finally, the term $\bar{v}$ is the velocity at which the shell-side fluid enters the bore-side sink. It therefore corresponds to the permeation velocity, J_w, given by Eq. (1). Under normal operating conditions the permeation velocity is about three orders of magnitude less than the bulk shell-side velocity. Hence, one may assume that

$$\bar{v} \ll v \tag{10d}$$

Substituting from Eqs. (10b)–(10c) into Eq. (10a), one obtains an identical expression to Eq. (9).

In general, the damping forces due to the flow parallel and normal to the fibers are different. This calls for the use of an anisotropic permeability tensor. Several models have been proposed for the estimation of Darcy's permeability of fibrous porous media (see Ref. 12 for a recent review). The application of these different models for typical HFRO units yields close results for the longitudinal and the transverse permeabilities. It is also worth noting that the characterization of fiber orientation as being parallel to the central axis of the shell is inexact. In fact, the flexible nature of the fibers suggests that the directional arrangement of the fiber bundle may be influenced by the shell-side flow. In this context the work of Spielman and Goren (29) presented an expression for a scalar permeability of fibrous media with random orientation. It is interesting to note that for typical HFRO modules, permeability values obtained through Spielman-and-Goren's expression are very close to those evaluated via the less involved model of Happel (10) for flow normal to an array of cylinders. Therefore, in our analysis a scalar permeability is assumed. In Eqs. (9) and (10b) the permeability of the medium, k, will be determined from the following expression derived by Happel (10) by applying the free-surface model to the problem of flow perpendicular to an array of cylinders

$$k = \frac{b_1^2}{4}\left[\ln\left[\frac{b_1}{r_0}\right] - \frac{1}{2}\left[\frac{b_1^4 - r_0^4}{b_1^4 + r_0^4}\right]\right] \tag{11a}$$

where the radius of the free-surface cell surrounding each fiber, b_1, is given by

$$b_1 = r_0/\sqrt{1 - \epsilon} \tag{11b}$$

Substituting from Eq. (11b) into Eq. (11a) and rearranging, we obtain

$$k = \frac{r_0^2}{8(1-\epsilon)}\left\{\ln\left[\frac{1}{1-\epsilon}\right] - \left[\frac{1-(1-\epsilon)^2}{1+(1-\epsilon)^2}\right]\right\} \tag{12}$$

Equation (9) is the governing equation of the shell-side hydraulics. Therefore, using Eq. (9) and assuming steady-state flow of a Newtonian fluid in a shell that is symmetric with respect to the angular coordinate (i.e., vanishing gradients with respect to angular coordinate), one may write the following "modified" Navier–Stokes equations:

z-component

$$\rho v_z \frac{\partial v_z}{\partial z} + \rho v_r \frac{\partial v_z}{\partial r} - \mu \frac{\partial}{\partial z}\left[\frac{\partial v_z}{\partial z}\right] - \frac{\mu}{r}\frac{\partial}{\partial r}\left[r\frac{\partial v_z}{\partial r}\right] + \left[\frac{\mu}{k} - \rho Q\right] v_z + \frac{\partial p_1}{\partial z} = 0 \tag{13}$$

with the boundary conditions

$$v_z(z, R_f) = 0 \tag{14}$$

$$v_z(z, R_S) = 0 \tag{15}$$

$$v_z(0, r) = 0 \tag{16}$$

$$v_z(L, r_f) = 0 \tag{17}$$

$$p_1(z, R_f) = p_f \tag{18}$$

r-component

$$\rho v_z \frac{\partial v_r}{\partial z} + \rho v_r \frac{\partial v_r}{\partial r} - \mu \frac{\partial}{\partial z}\left[\frac{\partial v_r}{\partial z}\right] - \mu \frac{\partial}{\partial r}\frac{1}{r}\left[\frac{\partial r v_r}{\partial r}\right] + \left[\frac{\mu}{k} - \rho Q\right] v_r + \frac{\partial p_1}{\partial r} = 0 \tag{19}$$

subject to the boundary conditions

$$v_r(z, R_f) = \frac{q_f}{2\pi R_f L} \tag{20}$$

$$\frac{\partial v_r(z, R_s)}{\partial r} = 0 \tag{21}$$

$$v_r(0, r) = 0 \tag{22}$$

$$v_r(L, r) = 0 \tag{23}$$

The set of Eqs. (13) through (23) provides a complete description of the shell-side hydraulics. It should be pointed out that owing to the coupling between the shell side and the bore side (as indicated by the existence of parameter Q in Eqs. 13 and 19, the foregoing set of equations should be solved simultaneously with the complete model for the bore side.

Component Continuity Equation for Salt in the Shell Side

In analyzing the salt convective-diffusion equation, Kabadi et al. (14) showed that under typical operating conditions radial convection dominates radial diffusion as the transport mechanism. Neglecting radial diffusion in comparison with convective flow, one can write

$$v_z \frac{\partial c_1}{\partial z} + v_r \frac{\partial c_1}{\partial r} - D \frac{\partial^2 c_1}{\partial z^2} + R_1 = 0 \tag{24}$$

where R_1 is the rate of salt mass permeated per unit shell volume and is given by

$$R_1 = \frac{2(1 - \epsilon)}{r_0} J_s \tag{25}$$

Equation (24) is subject to the following boundary conditions:

$$c_1(z, R_f) = c_f \tag{26}$$

$$\frac{\partial c_1(0, r)}{\partial z} = 0 \tag{27}$$

$$\frac{\partial c_1(L, r)}{\partial z} = 0 \tag{28}$$

Bore-Side Equations

Let us consider a hollow fiber that is located at a distance r from the central axis of the shell. The flow inside this fiber is represented by the flow in a hollow cylinder with a porous wall. Radial injection takes place through the porous wall of the cylinder via permeation. This problem was addressed by Yuan and Finkelstein (32) who tackled the problem of flow along a porous pipe with radial injection. For the case of small injection velocities, they derived a solution for the equations of motion via the method of perturbation. They have shown that at any given radial position inside the fibers, the axial variation in the pressure over a distance Δz (for which the permeation velocity is constant) is expressed by

$$\frac{\Delta p_3}{\Delta z} = -\frac{8\mu}{r_i^2} u_z(1 + 0.75\lambda - 0.041\lambda^2) \times \left[\frac{1}{1 - 0.056\lambda + 0.015\lambda^2} + \frac{\lambda\mu\Delta z}{\rho r_i^2 u_z}\right] \tag{29}$$

where

$$\lambda = \frac{\rho J_w r_i}{\mu} \tag{30}$$

and u_z is the average bore-side axial velocity at $z + \Delta z$.

Equation (29) is strictly valid for values of λ that are smaller than 1. In a typical HFRO experiment, λ range between 10^{-3} and 10^{-4}. It is interesting to note that when the permeation velocity is vanishingly small, Eq. (29) reduces to the Hagen–Poiseuille equation. Since the permeate leaves the unit at atmospheric pressure, Eq. (29) is subject to the following boundary condition

$$p_3(L, r) = p_{atm} + \Delta p_{sealing} \tag{31a}$$

where $\Delta p_{sealing}$ is the pressure drop of the permeate through the epoxy sealing ring as given by the Hagen–Poiseuille equation:

$$\Delta p_{sealing} = \frac{8\mu L_s}{r_i^2} u_z(L, r) \tag{31b}$$

Bore-Side Total Continuity Equations

The radial-averaged continuity equation inside the bore can be written as

$$\frac{\partial u_z}{\partial z} - Q\left[\frac{r_0^2}{r_i^2(1 - \epsilon)}\right] = 0 \tag{32}$$

with the boundary condition

$$u_z(0, r) = 0 \tag{33}$$

Component Continuity Equation for Salt

Material balance on salt around an element of fibers

$$\frac{d(u_z c_3)}{dz} = \frac{2r_0}{r_i^2} J_s \tag{34}$$

subject to the boundary conditions

$$c_3(0, r) = 0 \tag{35a}$$

Instead of Eq. (35a), a more formal boundary condition can be used; namely,

$$c_3(0, r) = J_s(0, r)/J_w(0, r) \tag{35b}$$

In either case, the selection of Eq. (35a) or (35b) does not alter the quantity of salt at $z = 0$ due to the boundary condition (33). In addition, the value of $c_3(0, r)$ is not an important parameter for the values of the subsequent rates of salt and water permeation for $z > 0$. This can be best explained by noting that in a typical HFRO experiment, the applied pressure is an order of magnitude higher than the osmotic pressure of the permeate. Furthermore, the shell-side concentration is typically an order of magnitude higher than the permeate concentration. Hence, by recalling Eqs. (2) and (3), one can show that whether Eq. (35a) or (35b) is employed, no tangible change is likely to occur. Nonetheless, due to the computational merits of Eq. (35a), it will be used in favor of Eq. (35b).

The derived set of partial differential equations describing the behavior of HFRO units can be solved numerically. The numerical discretization algorithm that we employed to solve the model equations is based upon transforming the differential equations of the model into discretized algebraic equations via a two-phase version of the semi-implicit method for pressure-linked equations "SIMPLE" (21). Additional details on the numerical algorithm can be found elsewhere (5).

RESULTS AND DISCUSSION

In this section the results of the devised mathematical model coupled with the proposed numerical algorithm will be investigated. First, the mathematical model will be employed along with published experimental data to evaluate the membrane-transport parameters. Toward this objective, the results of 115 experimental runs conducted by El-Halwagi (5), Ohya et al. (18), and Kabadi (13) are used in conjunction with the proposed model to estimate the values of the nine transport constants. In these three experimental works, Du-Pont B-9 HFRO modules were employed for pure water and NaCl–water systems. The inside and outside radii of these polyamide fibers are 21×10^{-6} and 42×10^{-6} m, respectively. Three different module sized [shell diameter (m) and active fiber length (m)] were used. These are (0.102 and 0.44), (0.114 and 1.22), and (0.114 and 0.75) in the works of El-Halwagi (5), Ohya et al. (18), and Kabadi (13), respectively. Following the estimation of membrane-transport parameters, the model validity will be tested via comparison with experimental data. Next, the model will be used to investigate the hydrodynamic performance of HFRO units. Finally, the computational requirements of the proposed numerical algorithm will be discussed.

Estimation of Membrane-Transport Parameters

The membrane-transport Eq. (1) and (4) contain three parameters: L_p, σ, and ω. In order that any mathematical model for the hydrodynamics of the HFRO system yields accurate results, the values of these three parameters ought to be known with a reasonable degree of accuracy. As has been observed by many investigators, the three parameters are dependent upon the operating pressures and concentrations (e.g., Refs. 4, 22, 23, and 26). The pressure dependence is normally attributed to membrane compaction whereas the influence of concentration can be explained by the phenomenon of membrane swelling. To account for this phenomenon, the three transport parameters were allowed to vary within the system according to the following expressions (which were found by several investigators to best fit the experimental data, e.g., Refs. 4 and 23):

$$L_p = L_{po} \exp\left[\alpha_1 \frac{(p_1 - p_3)}{p_{ref}}\right] \exp\left[\beta_1 \frac{c_1}{c_{ref}}\right] \tag{36}$$

$$\sigma = \sigma_0 \left[\frac{(p_1 - p_3)}{p_{ref}}\right]^{\alpha_2} \left[\frac{c_1}{c_{ref}}\right]^{\beta_2} \tag{37}$$

and

$$\omega = \omega_0 \left[\frac{(p_1 - p_3)}{p_{ref}}\right]^{\alpha_3} \left[\frac{c_1}{c_{ref}}\right]^{\beta_3} \tag{38}$$

where L_{po}, α_1, β_1, σ_0, α_2, β_2, ω_0, α_3, and β_3 are all assumed to be concentration and pressure-independent. p_{ref} and c_{ref} are taken as atmospheric pressure and 1 kg/m^3, respectively. Hence, the problem of estimating the three transport parameters becomes one of evaluating these nine constants.

In order to address the parameter-estimation problem, pure-water experimental data (5, 18) were first used to evaluate L_{po} and α_1.

The problem was tackled as a simple two-variable unconstrained minimization problem. The objective of this optimization program is to obtain the values of L_{po} and α_1 that minimize the sum of the squares of relative errors of the theoretically predicted permeate flow rates and concentrations from those observed experimentally. The gradients as well as the elements of the Hessian matrix were calculated numerically using centered finite difference schemes. By employing Newton's unconstrained optimization method iteratively, the following values were obtained:

$$L_{po} = 2.3 \times 10^{-13} \text{ m/spa}$$

$$\alpha_1 = -0.03$$

subsequently, a similar procedure was followed for evaluating the remaining transport parameters. The salt experimental data of Kabadi (13) and Ohya et al. (18) were employed in conjunction with the proposed model to estimate β_1, σ_0, α_2, β_2, ω_0, α_3, and β_3. A seven-variable unconstrained minimization problem was solved to yield

$$\beta_1 = -0.102$$

$$\sigma_0 = 0.96$$

$$\alpha_2 = -0.009$$

$$\beta_2 = -0.011$$

$$\omega_0 = 2.47 \times 10^{-15} \text{ s/m}$$

$$\alpha_3 = -0.016$$

$$\beta_3 = -0.041$$

The above values propose that both σ and ω are not strongly influenced by variations in operating pressures and/or concentrations. It is worth pointing out that the above results are strictly confined to the water–salt system. For any other solute or solvent the corresponding experimental data ought to be employed along with the mathematical model to yield the appropriate transport parameters.

Model Validation

In order to assess the validity of the mathematical model as well as the values of the transport parameters, experimental data (other than those used for transport-parameters estimation) were invoked. As can be seen from Figs. 2–5, the model predictions agree with the experimental data (the model results are shown by the lines whereas the experimental data are represented by the geometrical symbols). In Fig. 2 the model results are compared with some of the experimental data reported by El-Halwagi (5) for pure-water experiments. It is worth noting that the decline in the permeate flow rate can be attributed to the reduction in transmembrane pressure-driving force. This reduction in driving force results from using a lower feed pressure or encountering higher frictional losses due to the increase in feed flow rate. Figure 3 also shows the theoretical versus the experimental results for pure-water experiments of Ohya et al. (18). The applied feed pressure for all the points in Fig. 3 is 2.4312×10^6 N/m^2. Next, the model was used to simulate the HFRO unit of Kabadi (13) under the conditions given in Figs. 4 and 5. Again, the agreement between the model results for the permeate flow rate and concentration with the experimental data confirms the model validity.

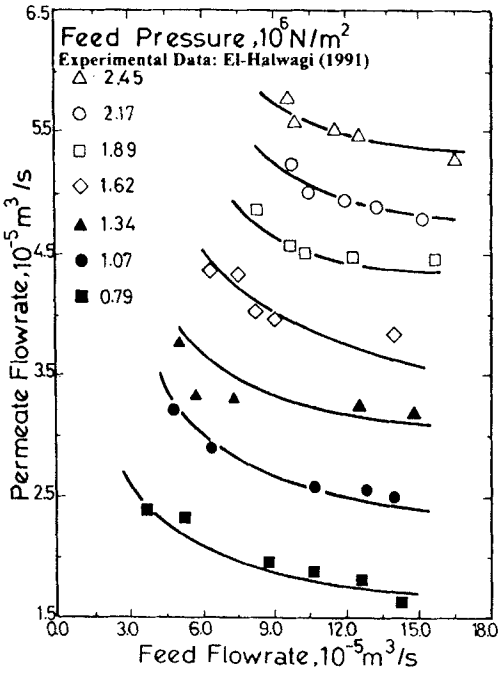

FIG. 2 Theoretical predictions versus experimental data (5) for pure-water experiments.

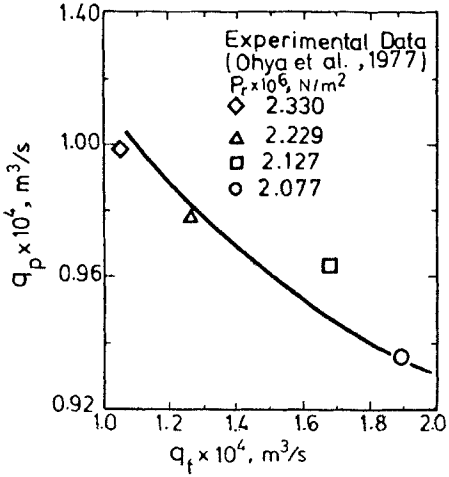

FIG. 3 Theoretical results and experimental data (18) for pure water experiments.

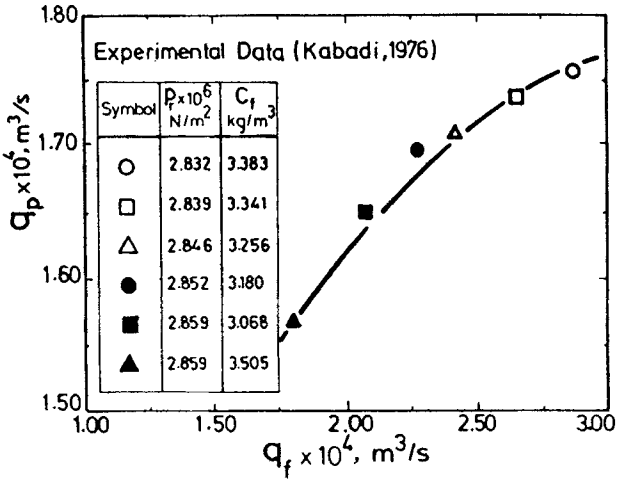

FIG. 4 Theoretical and experimental (13) permeate flow rate vs feed flow rate.

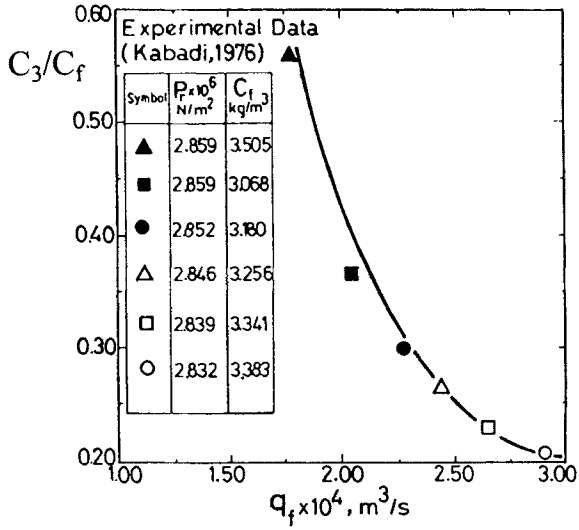

FIG. 5 Theoretical and experimental (13) permeate concentration vs feed flow rate.

Analysis of Transport Properties of HFRO Units

In this section the various mass- and momentum-transport characteristics for the shell and the bore fluids will be discussed. Figures 6–12 demonstrate the pressure, velocity, and concentration distributions in both phases as predicted by the proposed model. The input data in these figures are as follows $p_f = 2{,}431{,}200.0$ N/m^2, $p_r = 2{,}076{,}650.0$ N/m^2, $q_f = 1.728 \times 10^{-4}$ m^3/s, $q_r = 7.61 \times 10^{-5}$ m^3/s, $c_f = 3.50$ kg/m^3, $L_s = 1.22$ m, and $R_s = 0.114$ m. These data correspond to one of the experimental points of Ohya et al. (18). The theoretically predicted flow rates and concentrations for the permeate and the reject agree with those experimentally observed by Ohya et al. (18). The dimensionless radius, Y, is defined as

$$Y = (r - R_f)/(R_s - R_f) \tag{39}$$

Figure 6 illustrates the theoretical results for shell-side pressure profiles throughout the unit. The model predictions indicate that, indeed, significant pressure variations throughout the shell side can take place. Such variations contribute toward the change of the other hydrodynamic variables throughout the HFRO module.

Figure 7 shows the shell-side radial velocity distribution. While v_r decreases monotonically in the radial direction (by virtue of permeation and increasing flow area), its value exhibits a nonmonotonic behavior in the

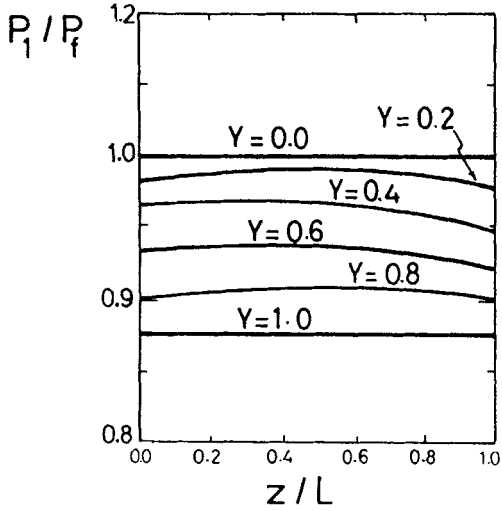

FIG. 6 Shell-side pressure distribution.

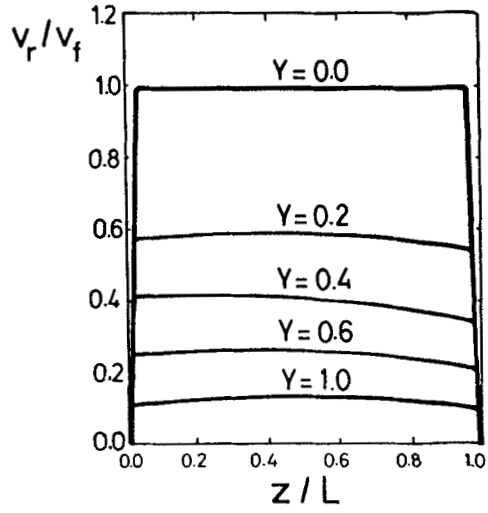

FIG. 7 Shell-side radial-velocity distribution.

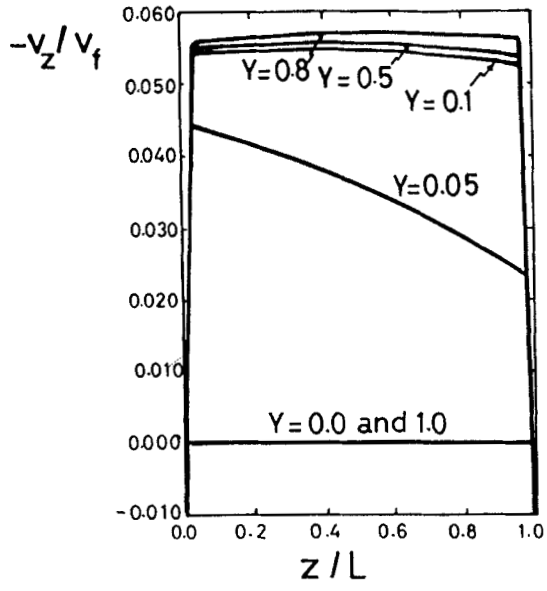

FIG. 8 Shell-side axial-velocity distribution.

radial direction. This is attributed primarily to the nonmonotonic change in the permeation rate which is a function of the shell-side pressure and concentration as well as the bore-side pressure and concentration.

In Fig. 8 the model results indicate that indeed a horizontal shell-side velocity component is generated. Although in this figure the axial velocity is negative (namely it flows left with respect to Fig. 1), yet depending upon the pressure distribution and the rate of permeation, the magnitude and direction of this velocity may vary significantly.

Figure 9 demonstrates the shell-side concentration profiles. The nonmonotonic behavior results mainly from the relative rates of water and salt permeation. As the water flux increases with respect to the salt flux, the shell-side concentration increases and vice versa.

In Fig. 10 the bore-side pressure distribution is shown. The considerable axial variation in p_3 leads to varying rates of permeation along the hollow fiber. Clearly, any model that does not account for such a pressure drop overestimates the driving force of permeation. The bore-side velocity distribution is demonstrated in Fig. 11. Owing to the continuous water permeation along the fibers, the bore-side velocity increases nonmonotonically.

In Fig. 12 the bore-side concentration profiles are shown. While in this figure the concentration increases axially, yet it has to be borne in mind that depending on the relative permeation rates of the salt and water, the value of c_3 may decrease or increase axially.

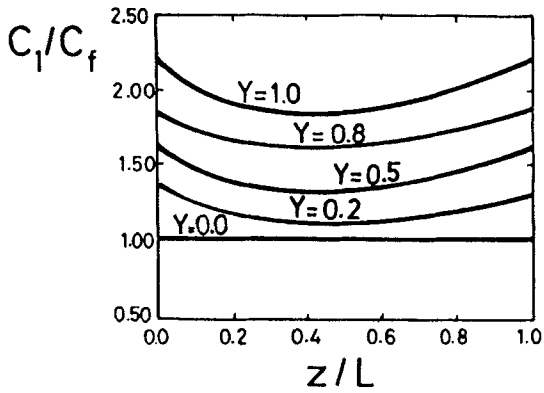

FIG. 9 Shell-side concentration profiles.

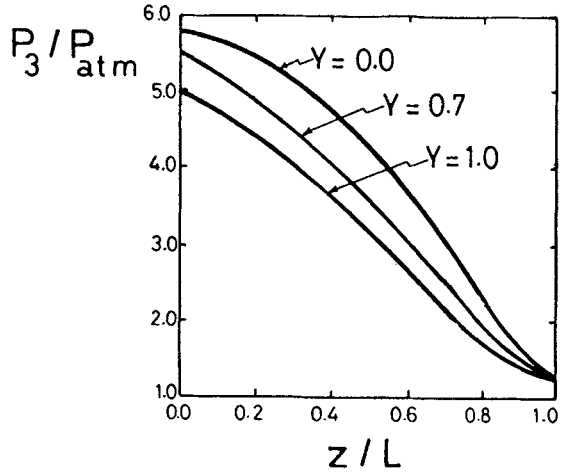

FIG. 10 Bore-side pressure profiles.

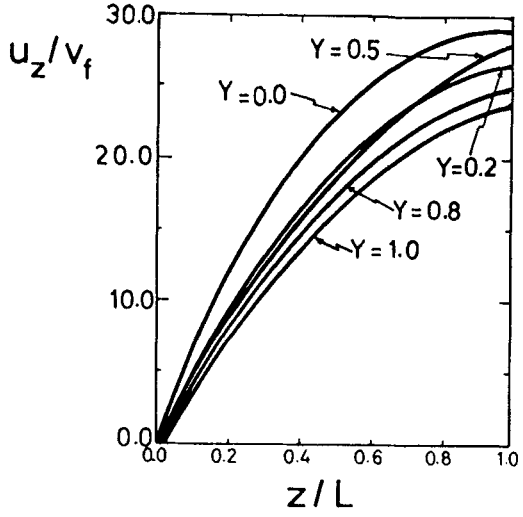

FIG. 11 Bore-side velocity distribution.

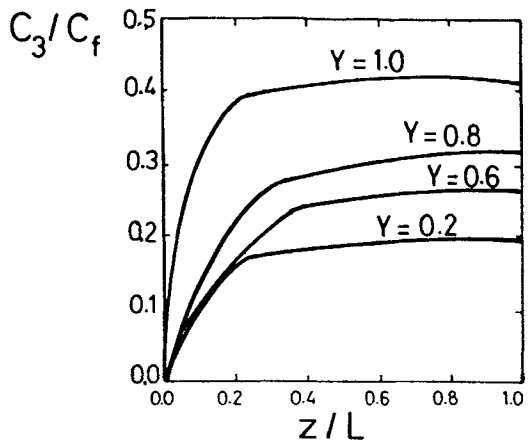

FIG. 12 Bore-side concentration profiles.

Computational Requirements

As has been previously mentioned, a numerical algorithm was developed to solve the model equations. This is based on the SIMPLE technique (16, 20, 21, 25). A Fortran program was developed to tackle the problem (5). The program was executed on a Sun Sparcstation 10 computer. In general, no convergence problems were observed when the system was discretized into a number of main grid points that is larger than 10×10. For mesh points less than that, divergence was commonly encountered. In general, a discretization grid of 50×50 points was found to be convenient both in terms of error and rate of convergence. For the majority of the input data, convergence was achieved within 10 iterations and in time less than 25 CPU seconds.

CONCLUSIONS AND RECOMMENDATIONS

Based upon the fundamental transport equations, a novel two-phase model was developed to describe the concentration, pressure, and velocity distributions in the shell and the bore sides of radial-flow hollow-fiber reserve-osmosis units. The devised momentum and mass transfer equations were coupled with the membrane transport equation to provide a complete description of these systems. This set of coupled nonlinear partial differential equations was transformed into discretized algebraic equa-

tions and solved numerically. For the majority of the input data, convergence was achieved in less than 10 iterations. Experimental data combined with the devised model were employed to obtain correlations for the dependence of the membrane-transport coefficients on pressure and concentration for the sodium chloride–water system. While the water permeability was found to be a strong function of the operating pressure and concentration, the reflection coefficient and the solute permeability have shown only a weak dependence on pressure and concentration. The experimental data were also used to assess the predictive power of the proposed model. The model validity was demonstrated through the agreement between the theoretical results with the experimental data. The model can, therefore, be reliably used in analyzing the behavior of hollow-fiber reverse-osmosis systems, particularly for transport-parameters estimation, scale-up, synthesis, and optimization purposes.

Owing to the growing interest in HFRO for environmental applications, the developed model can be used to predict the transport properties of various pollutants through membranes. While the correlations developed for L_p can be used for aqueous wastes, the correlations developed for σ and ω are only applicable to the NaCl–water system. Upon the availability of lab-scale experimental results on the separation of wastes using HFRO, the model can be employed to develop correlations for σ and ω in a similar manner to how this work has addressed the NaCl–water system. Another potential use of the model is in the area of process design and optimization. The model developed in the present work can be employed as a useful tool for establishing a systematic framework for optimizing the design of new HFRO systems and improving the performance of already existing units. This objective can be accomplished by incorporating the model into procedures for synthesis of optimal HFRO networks (e.g., Refs. 6 and 7). In this context the model is used to relate the performance of HFRO units to various operating and design parameters while the synthesis procedure steers the solution toward identifying the optimal conditions and system configuration.

SYMBOLS

b_1	radius of free-surface cell surrounding each fiber (m), defined by Eq. (11b)
B	damping force per unit volume of the shell that the outside surface of the fibers exerts on the shell-side fluid (N/m^3)
c_1	shell-side concentration (kg/m^3)

c_3	bore-side concentration (kg/m^3)
$(c_s)_{\text{log mean}}$	logarithmic mean solute concentration difference across the membrane
c_f	feed concentration (kg/m^3)
c_{ref}	reference concentration, taken as 1.0 kg/m^3
D	molecular diffusivity (m^2/s)
J_s	flux of solute across the membrane (kg/m^2·s)
J_w	water diffusive flux (m/s)
k	permeability of the shell side, defined by Eq. (12) (m^2)
L	active length of fiber (m)
L_p	filtration coefficient (m/Pa·s)
L_{po}	constant in Eq. (36) (m/Pa·s)
L_s	length of the epoxy sealing ring (m)
p_{atm}	atmospheric pressure (N/m^2)
P_f	feed pressure (N/m^2)
P_{ref}	reference pressure, taken as 1.013×10^5 N/m^2
P_1	shell-side pressure (N/m^2)
P_3	bore-side pressure (N/m^2)
q_f	feed volumetric flow rate (m^3/s)
q_p	permeate volumetric flow rate (m^3/s)
Q	permeation rate; volume of fluid entering the sink per unit shell volume per unit time (s^{-1})
r	radial coordinate
r_i	inside fiber radius (m)
r_o	outside fiber radius (m)
R_1	rate of salt consumed in unit shell volume (kg/m^3·s)
R_f	outside radius of the central feed (m)
R_s	inside radius of the shell (m)
S	mass rate of consumption of the shell-side fluid per unit shell volume, defined by Eq. (10c) (kg/m^3·s)
t	time (s)
u	linear velocity of the pore fluid (m/s)
u_r	bore-side velocity in the r-direction (m/s)
u_z	bore-side velocity in the z-direction (m/s)
v	shell-side velocity (m/s)
v_f	feed velocity (m/s)
v_r, v_x, v_y, v_z	r-, x-, y-, and z-components, respectively, of shell-side velocity (m/s)
$\bar{v}$	velocity at which the shell-side fluid enters the bore-side sink (m/s)
x	x-axial coordinate (m)
y	y-axial coordinate (m)

z	z-axial coordinate (m)
Y	dimensionless radius, defined by Eq. (39)

Greek Symbols

α_1	constant in Eq. (36)
α_2	constant in Eq. (37)
α_3	constant in Eq. (38)
β_1	constant in Eq. (36)
β_2	constant in Eq. (37)
β_3	constant in Eq. (38)
Δp	applied pressure difference across the membrane (N/m^2)
$\Delta p_{\text{sealing}}$	pressure drop inside the fiber through the epoxy sealing ring, defined by Eq. (31b) (N/m^2)
Δp_3	pressure drop inside the fiber over a distance Δz (N/m^2)
Δr	grid spacing in the r-direction (m)
Δz	grid spacing in the z-direction (m)
$\Delta\pi$	osmotic pressure difference across the membrane (N/m^2)
λ	dimensionless parameter, defined by Eq. (30)
ϵ	porosity of fiber bundle
μ	fluid dynamic viscosity (kg/m·s)
π	osmotic pressure (N/m^2)
ρ	fluid density (kg/m^3)
σ	reflection coefficient
σ_0	constant in Eq. (37)
ω	solute permeability at zero volume flux, defined by Eq. (4)
ω_0	constant in Eq. (38) (s/m)
τ	shear stress exerted on fluid (N/m^2)

Subscripts

1	shell side
3	bore side
r	r-direction
z	z-direction

REFERENCES

1. H. C. Brinkman, "A Calculation of the Viscous Force Exerted by a Flowing Fluid on a Dense Swarm of Particles," *Appl. Sci. Res.*, *A1*, 27–34 (1947).

2. Comb, L. F., "Going Forward with Reverse Osmosis," *Chem. Eng.*, pp. 90–92 (July 1994).
3. Dandavati, M. S., M. R. Doshi, and W. N. Gill, "Hollow Fiber Reverse Osmosis: Experiments and Analysis of Radial Flow Systems," *Chem. Eng. Sci., 30*, 877–886 (1975).
4. Dickson, J. M., T. Matsuura, P. Blais, and S. Sourirajan, "Some Transport Characteristics of Aromatic Polyamide Membranes in Reverse Osmosis," *J. Appl. Polym. Sci., 20*, 1491–1499 (1976).
5. El-Halwagi, A. M., "Mathematical Modeling and Experimental Investigation of Hollow-Fiber Reverse-Osmosis Systems," M.S. Thesis, University of California, Los Angeles, 1991.
6. El-Halwagi, M. M., "Synthesis of Reverse Osmosis Networks for Waste Reduction," *AIChE J., 38*(8), 1185–1198 (1992).
7. El-Halwagi, M. M., "Optimal Design of Membrane Hybrid Systems for Waste Reduction," *Sep. Sci. Technol., 28*(1–3), 855–872 (1993).
8. Gill, W. N., and B. Bansal, "Hollow Fiber Reverse-Osmosis Systems Analysis and Design," *AIChE J., 19*(4), 823–831 (1973).
9. Gupta, S. K., "Design and Analysis of a Radial-Flow Hollow-Fiber Reverse-Osmosis System," *Ind. Eng. Chem. Res., 26*, 2319–2323 (1987).
10. Happel, J., "Viscous Flow Relative to an Array of Cylinders," *AIChE J., 5*(2), 174–177 (1959).
11. Hermans, J. J., "Physical Aspects Governing the Design of Hollow Fiber Modules," *Desalination, 26*, 45–62 (1978).
12. Jackson, G. W., and D. F. James, "The Permeability of Fibrous Porous Media," *Can. J. Chem. Eng., 64*, 364–374 (1986).
13. Kabadi, V. N., "Reverse Osmosis in Hollow Fiber Radial Flow," M.S. Thesis, State University of New York at Buffalo, 1976.
14. Kabadi, V. N., M. R. Doshi and W. N. Gill, "Radial Flow Hollow Fiber Reverse Osmosis: Experiments and Theory," *Chem. Eng. Commun., 3*, 339–365 (1979).
15. Kedem, O., and A. Katchalsky, "Thermodynamic Analysis of the Permeability of Biological Membranes to Non-Electrolytes," *Biochim. Biophy. Acta, 27*, 229 (1958).
16. Kelkar, K. M., and S. R. Patankar, "Development of Generalized Block Correction Procedures for the Solution of Discretized Navier–Stokes Equations," *Comput. Phys. Commun., 53*, 329–336 (1989).
17. Lundgren, T. A., "Slow Flow through Stationary Random Beds and Suspensions of Spheres," *J. Fluid Mech., 51*(2), 273–299 (1972).
18. Ohya, H., H. Nakajima, K. Takagi, S. Kagawa, and Y. Negishi, "An Analysis of Reverse Osmotic Characteristics of B-9 Hollow Module," *Desalination, 21*, 257–274 (1977).
19. Orofino, T. A., "Technology of Hollow Fiber Reverse Osmosis Systems," in *Reverse Osmosis and Synthetic Membranes* (S. Sourirajan, Ed.), National Research Council Canada, Ottawa, 1977, pp. 313–341.
20. Patankar, S. V., "Numerical Prediction of Three-Dimensional Flows," in *Studies in Convection: Theory, Measurement and Applications, Vol. 1*, (B. E., Launeutte Ed.), Academic Press, New York, NY, 1975.
21. Patankar, S. V., *Numerical Heat Transfer and Fluid Flow*, McGraw-Hill, New York, NY, 1981.
22. Pusch, W., "Transport Behavior of Asymmetric Polyamide Flat Sheet Membranes and Hollow Fine Fibers in Dialysis-Osmosis and Hyperfiltration and Ultrafiltration Membranes and Applications," *Polym. Sci. Technol., 13*, 129–140 (1979).

23. Rautenbach, R., and R. Albrecht, *Membrane Processes*, Wiley, New York, NY, 1989.
24. Rorech, G. J., and S. G. Bond, "Reverse Osmosis: A Cost Effective Versatile Water Purification Tool," *Ind. Eng. Chem.*, pp. 35–37 (November 1993).
25. Smith, G. D., *Numerical Solution of Partial Differential Equations: Finite Difference Methods, 3rd ed.*, Clarendon Press, Oxford, 1985, pp. 24–25.
26. Soltanieh, M., and W. N. Gill, "Review of Reverse Osmosis Membranes and Transport Models," *Chem. Eng. Commun.*, *12*, 279–363 (1981).
27. Soltanieh, M., and W. N. Gill, "Analysis and Design of Hollow Fiber Reverse Osmosis Systems," *Ibid.*, *18*, 311–330 (1982).
28. Soltanieh, M., and W. N. Gill, "An Experimental Study of the Complete Mixing Model for Radial Flow Hollow Fiber Reverse Osmosis Systems," *Desalination*, *49*, 57–88 (1984).
29. Spielmen, L., and S. L. Goren, "Model for Predicting Pressure Drop and Filtration Efficiency in Porous Media," *Environ. Sci. Technol.*, *2*, 279–287 (1968).
30. Tam, C. K., "The Drag on a Cloud of Spherical Particles in Low Reynolds Number Flow," *J. Fluid Mech.*, *38*(3), 537–546 (1969).
31. Whitaker, S., "Transport Processes with Heterogeneous Reaction," in *Concepts and Design of Chemical Reactors* (S. Whitaker and A. L. Cassano, Eds.), Gordon and Breach Science Publisher, New York, NY, 1986, pp. 1–9.
32. Yuan, S. W., and A. B. Finkelstein, "Laminar Pipe Flow with Injection and Suction through a Porous Wall," *Trans. ASME*, *78*, 719–724 (1956).

Received by editor September 18, 1994
Revision received April 6, 1995